## CONFERENCE PRE-PRINT

# DEFINING OPERATIONAL SCENARIOS FOR DTT IN METALLIC ENVIRONMENT: A MODELING STUDY OF CORE-EDGE DYNAMICS AND PLASMA-WALL INTERACTION

L. BALBINOT DTT Scarl

Frascati, Rome, Italy

Email: luca.balbinot@dtt-project.it

G. ALBERTI Organization Milan, Italy

N. BONANOMI

Max Planck Institute for Plasma Physics

Garching, Germany

F. CANI

Istituto per la Scienza e Tecnologia dei Plasmi-CNR Milano, Italy

R. AMBROSINO CREATE-ENEA Napoli, Italy

I. CASIRAGHI

Istituto per la Scienza e Tecnologia dei Plasmi-CNR

Milano, Italy

A. CASTALDO ENEA, C.R. Frascati

Frascati, Rome, Italy

P. MANTICA

Istituto per la Scienza e Tecnologia dei Plasmi-CNR

Milano, Italy

C. MEINERI

Dipartimento Energia, Politecnico di Torino

Torino, Italy

M. PASSONI

Politecnico di Milano and Istituto per la Scienza e

Tecnologia dei Plasmi-CNR

Milano, Italy

G. RUBINO

Istituto per la Scienza e la Tecnologia dei Plasmi, CNR

Bari, Italy

P. INNOCENTE

Istituto per la Scienza e Tecnologia dei Plasmi, CNR

Padova, Italy

# Abstract

The Divertor Test Tokamak (DTT), under construction in Frascati, is designed to explore power exhaust and plasma-wall interaction in multiple divertor configurations during its operational life. The first wall, including the divertor, will be fully tungsten-clad. This paper describes three reference scenarios, spanning plasma currents from 3 to 5.5 MA, toroidal fields from 29 to 5.85 T, and auxiliary heating powers from 8 to 45 MW, covering ramp-up, L-mode and H-mode phases. Integrated modelling was applied using METIS for ramp-up estimation, ASTRA for core transport, CREATE-NL for equilibria and control, SOLEDGE2D-EIRENE for edge plasma and wall loading, and ERO2.0 for tungsten sputtering. Particular attention was given to edge plasma physics, which couples core and Plasma-Wall Interaction (PWI) modelling and provided essential input for divertor design. Transport coefficients were assigned based on plasma phase, combining empirical scalings and model outputs, with deviations increasing at high magnetic fields. Results show that limiter and wall temperatures, impurity sources and tungsten concentrations remain within experimental ranges, though limiter temperatures above 100 eV may appear in the highest-power case for a few seconds. Optimisation of the ramp-up phase is critical to control loop voltage and limit tungsten sources, as impurity accumulation can hinder the L-H transition. PWI modelling indicates that the proposed ramp-up and flat-top schemes, together with the reference geometry, ensure low plasma contamination and acceptable erosion within the expected component lifetime. Analysis of alternative limiter geometries confirms that optimisation can mitigate impurity sources while remaining consistent with core transport. The study demonstrates that well-designed scenarios allow DTT to meet its performance targets while addressing plasma-wall interaction in a metallic device, providing a platform for ITERand DEMO-relevant investigations.

#### 1. INTRODUCTION

The Divertor Tokamak Test facility (DTT) is a next-generation superconducting tokamak under construction in Frascati, Italy, specifically designed to investigate power exhaust solutions for future fusion reactors[1][2]. With a major radius of  $R_0$  = 2.19 m, minor radius a= 0.7 m, maximum plasma current  $I_p$  = 5.5 MA and toroidal field  $B_T$  = 5.85 T, DTT will provide reactor-relevant conditions in terms of P/R<sub>0</sub> and edge power fluxes, in a fully metallic environment. The device will be equipped with up to 45 MW of auxiliary heating, combining Electron Cyclotron Resonance Heating (ECRH), Neutral Beam Injection (NBI) and Ion Cyclotron Resonance Heating (ICRH), and with a tungsten divertor featuring advanced geometries such as single null, double null, negative triangularity and super-X.

A key challenge for DTT is the development of stationary scenarios that ensure simultaneous control of the plasma core, pedestal, and Scrape-Off Layer (SOL), while mitigating impurity accumulation and limiting wall sputtering. This is especially critical in a full-metal environment, where plasma-wall interaction can strongly influence confinement and radiative losses as demonstrated in WEST[3]. For this reason, the definition of operational scenarios necessitates an integrated approach that couples core transport, edge physics, and plasma-wall interaction.

DTT will operate with different plasma parameters during its lifespan. In this paper, the focus is on the principal Single-Null (SN) inductive scenario whose characteristics are listed in Tab. 1[4][5]. Scenario A represents the initial stage of DTT operation, designed to explore plasma behaviour at reduced current and magnetic field, relying solely on ECRH as the heating system. Although less demanding in terms of performance, this scenario provides valuable insight into plasma control with extended discharge durations. Scenario E corresponds to the most demanding configuration foreseen for DTT, aiming to test operation under reactor-relevant conditions having a P/R factor close to DEMO's [6]; it will require high-density seeded operation to be safely operated.

TABLE 1. LIST OF RELEVANT PLASMA PARAMETERS FOR MAIN DTT SN SCENARIOS.

	I <sub>p</sub> (MA)	$B_{T}(T)$	$P_{aux}(MW)$	$\bar{n}_e~(\mathrm{m}^{-3})$	$\bar{T}_e$ (keV)	$n_{e,sep} (m^{-3})$
Scenario A	2	3	7.2	$9 \times 10^{19}$	5	$3.5 \times 10^{19}$
Scenario C	4	5.85	20.2	$14 \times 10^{19}$		$5.0 \times 10^{19}$
Scenario E	5.5	5.85	45	$19 \times 10^{19}$	12	$8.0 \times 10^{19}$

In this work, time-dependent integrated modelling is employed to explore the evolution of plasma profiles in the main DTT scenarios, focusing on the interplay between confinement, pedestal stability, plasma control, core and edge transport, SOL conditions and plasma-wall interaction (PWI). The aim is to identify operational windows that combine high performance (in terms of density, temperature and energy confinement) with acceptable impurity and heat loads on plasma-facing components. The actuators are: ramp-up scheme (density,  $P_{aux}$  and  $I_P$ ), plasma and wall shape. The analysis includes the description of the identified heating schemes and plasma configurations, aiming at defining robust discharge trajectories from ramp-up to H-mode operation. The integrated modelling approach was crucial in the machine design process to identify and correct or optimise features that could affect machine performance, like heating schemes or divertor and first wall geometry.

The paper is structured as follows: section 2 describes the overall methodology modeling tools; section 3 core modelling results with emphasis on core-edge coupling constraints; section 4 discusses edge modelling methodology and results and implications for power exhaust strategies in DTT; section 5, plasma-wall interaction modelling is described; conclusions are drawn in section 6.

## 2. METHODOLOGY

Current core, edge, or PWI plasma modelling codes require multiple assumptions, input parameters, and interdependent boundary conditions. For example, the edge plasma provides temperature and density to the LCFS to the core codes and the entire background plasma to the PWI codes, which can estimate the source of impurities that directly affect the core and edge. The use of these codes, therefore, requires strong assumptions derived from experimental data or, in the case of machines under construction, from careful integrated modelling, a very long iterative process.

The definition of plasma parameters during ramp-up and flat top for scenarios A and E was developed to reduce  $V_{loop}$  consumption, facilitated by low densities and high temperatures, and minimising tungsten erosion, a condition achievable at high densities and low temperatures.

Given the high densities at which the machine will operate, the fastest possible ramp-up scheme was developed with the CREATE-NL[7] code to allow plasma controllability with the applied technologies and DTT design. This

scheme was used in the initial core modelling performed with METIS[8] that verifies the use of  $V_{loop}$  using multiple boundary conditions calculated using simple models such as the two-point model[9] and Eich's scaling [10] or Scarabosio's scaling[11] for the H-mode and L-mode divertor phases respectively, and Goldston's empirical model [12] for the limiter phase.

Once a ramp-up scheme was obtained, self consistent core modelling was performed with ASTRA[13][14] to estimate the transport (including transport parameters and pinch effects) and performance of the machine in different operating scenarios (Sec. 3). This allowed the estimation of energy and particle fluxes and transport parameters that were used for the edge simulations performed with SOLEDGE2D-Eirene[15][16] (Sec. 4). These simulations validated boundary conditions assumed in ASTRA modelling, estimated the fluxes and temperatures at the first wall at different times in the various scenarios and provided the background plasma for the PWI simulations carried out with ERO2.0[17] (Sec. 5). The latter estimated the influx and concentration of tungsten at different times and operating scenarios and thus validated the assumptions made in the plasma core modelling.

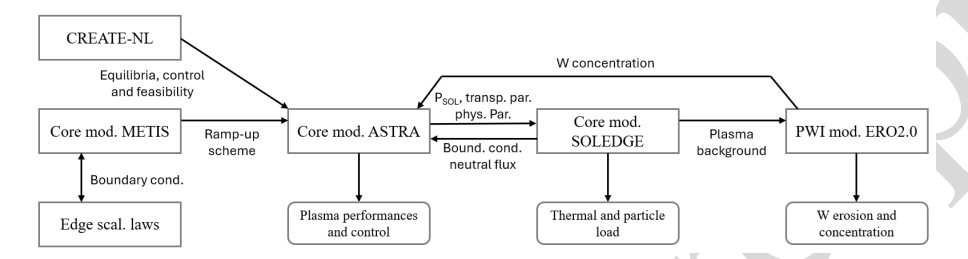


FIG. 1. Scheme of the integrated modelling methodology applied; squared boxes represent tools, rounded boxes indicate modelling outputs.

The methodology applied is summarised in the descriptive diagram shown in Fig. 1. Overall, the methodology provides a comprehensive framework to quantify erosion rates, impurity migration pathways, and the resulting core contamination during DTT operation, highlighting the coupling between plasma boundary conditions, material response, and impurity transport physics.

#### 3. CORE MODELLING

The simulations were mainly conducted using the ASTRA transport code, coupled with reduced models for turbulent, neoclassical and impurity transport. In particular, TGLF-SAT2 was used for quasi-linear turbulent transport, NCLASS for neoclassical transport, FACIT for neoclassical impurity transport, while IMEP routines were used to calculate the pedestal in H-mode. The simulations cover the entire confined plasma radius, from the initial limiter phase to the flat-top in H-mode. The profiles of electron and ion temperature, electron density, density of two impurity species and plasma current are evolved as a function of time. The boundary conditions are regulated by neutral flow controls and impurity sources to maintain realistic levels of density and radiated power. The effect of the radial electric field, sawtooth instabilities and the L-H transition (according to Martin scaling) are included. Auxiliary powers are modelled with depositions calculated by dedicated routines (RABBIT for NBI, PION or Gaussian for ICRH, Gaussian for ECRH).

To reduce computation time and test the robustness of the scenarios, the METIS code, an integrated "0.5D" model, was also used. Profiles, boundary conditions and global parameters could be lightly coupled with simple power exhaust estimations, such as the first wall of the last closed flux surface (LCFS) plasma temperature derived from scaling. Compared to ASTRA, METIS adopts a simplified approach: current diffusion is solved with a reduced grid, while heat transport is treated with a combination of 0D–1D models, in which temperature profiles are reconstructed from scaling laws for energy confinement time. Power depositions are described with Gaussian profiles calibrated on ASTRA results, while densities follow prescriptive forms (line-averaged density, peaking factor and separatrix value). Impurities are treated in a simplified manner by imposing fixed values of  $Z_{\rm eff}$  and species ratios derived from existing experiments. These values are validated by edge and PWI modelling.

This combined strategy allows, on the one hand, detailed and physically consistent predictions with ASTRA and, on the other, a rapid exploratory tool with METIS to optimise scenarios and compare results in terms of flux consumption. A complete description of core modelling methodology and results is given in [4][5].

## 3.1. Scenario A results

Results relative to Scenario A ramp-up and flat top are described in this section. The L–H transition takes place at about  $t\simeq 5.2$  s, with a threshold power  $P_{\rm L-H}\simeq 5$  MW, achieved at  $\bar{n}e/n_G\simeq 0.45$ . The pedestal is characterized

by  $T_{e,ped} \simeq T_{i,ped} \simeq 1.2\,\mathrm{keV}$  and  $n_{e,ped} \simeq 8.2 \times 10^{19}, \mathrm{m}^{-3}$ . Central values in the H-mode phase are  $T_e(0) \simeq 5\,\mathrm{keV}$ ,  $T_i(0) \simeq 3.5\,\mathrm{keV}$ , and  $n_e(0) \simeq 1.2 \times 10^{20}, \mathrm{m}^{-3}$ .

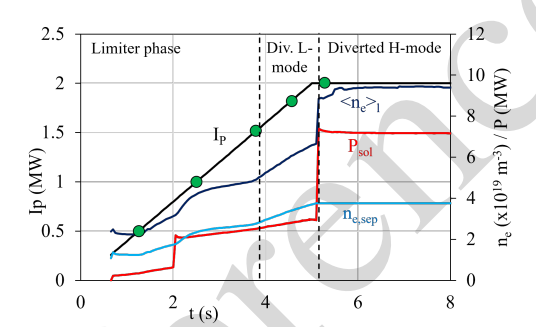
The magnetic flux consumption is limited to  $\sim 5$  Vs at the L-H transition, against a total solenoid availability of 25.5 Vs, which allows for a flat-top lasting over 100 s. Both  $l_{i3}$  and  $\beta_{pol}$  remain comfortably within control ranges. Radiation losses, modelled as 25% of the injected power with nitrogen and tungsten impurities included, do not compromise the stability of the profiles nor the sustainment of the long discharge. Ramp-up of main plasma variables is shown in Fig. 2a; vertical dashed lines separate limiter, diverted L-mode and diverted H-mode phases

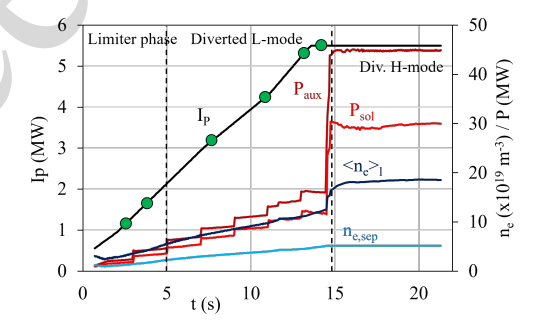
#### 3.2. Scenario E results

Scenario E corresponds to the most demanding configuration foreseen for DTT, aiming to test operation under reactor-relevant conditions and requiring the greatest compromise to establish a suitable operational regime. ASTRA simulations indicate that the sequence of current ramp-up, L-H transition, and flat-top can be successfully sustained, provided auxiliary heating is carefully managed to control current profiles and magnetohydrodynamic stability.

During the ramp-up, electron cyclotron heating (ECRH) is applied with a mix of on- and off-axis deposition to avoid excessive peaking of the current profile and to limit the rise of the internal inductance ( $l_{i3}$ ). This strategy reduces the risk of sawtooth instabilities and helps maintain  $\beta_{\rm pol}$  within the operational window. The L–H transition occurs at approximately  $t\simeq 14.5$  s, with a threshold power  $P_{\rm L-H}\simeq 15.5$  MW, consistent with the Martin scaling. Once in H-mode, the pedestal reaches values of  $T_{e,\rm ped}\simeq 3.2$  keV,  $T_{i,\rm ped}\simeq 3.2$  keV, and  $n_{e,\rm ped}\simeq 1.2\times 10^{20}$ , m<sup>-3</sup>. In the flat-top, central parameters are  $T_e(0)\simeq 12$  keV,  $T_i(0)\simeq 9$  keV, and  $n_e(0)\simeq 2.2\times 10^{20}$ , m<sup>-3</sup>, with a lineaveraged density corresponding to  $\bar{n}e/n_G\simeq 0.45$ . The global performance metrics are  $\beta_N\simeq 1.6$ ,  $H_{98}\simeq 0.9$ , while both  $I_{i3}$  and  $\beta_{\rm pol}$  remain within acceptable limits. The achievable flat-top duration is estimated in the range 20–30 s, extendable to about 40 s if a faster ramp-up rate ( $\sim 600$  kA/s) is adopted, which lowers the consumption of magnetic flux from the central solenoid.

Comparisons with METIS (a faster 0.5D transport model) and with equilibrium analyses from CREATE-NL+ confirm the feasibility of Scenario E, with only modest discrepancies in  $l_{i3}$ ,  $\beta_{pol}$ , and flux consumption. Ramp-up of main plasma variables is shown in Fig. 2a





- (a) Scenario A ramp-up and flat top scheme.
- (b) Scenario E ramp-up and flat top scheme.

FIG. 2. Scenario A and Scenario E ramp-up and start of flat-top schemes, green dots indicate the instant selected for edge modelling.

# 4. EDGE MODELLING

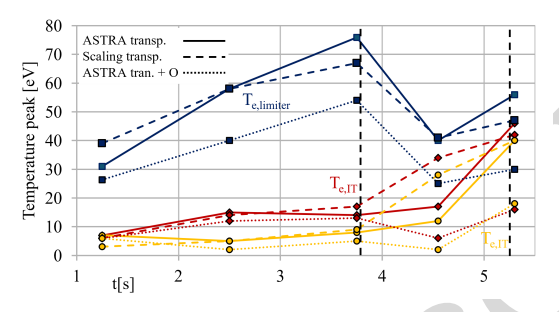
Edge modelling was performed with SOLEDGE2D-Eirene using ASTRA output as input parameters.

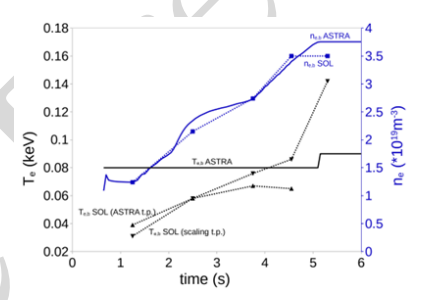
Ramp-up phases of scenarios A and E were investigated at representative time slices indicated by green dots in figure 4, covering limiter, L-mode, L-H transition, and flat-top conditions. Input equilibria and separatrix parameters were derived from ASTRA. Two approaches were used to define edge transport coefficients: (i) direct extraction from ASTRA near the separatrix, and (ii) empirical  $\lambda_q$  scalings. Double  $\lambda_q[18]$  was considered for limiter phase separating near SOL[12] from far SOL[19], an L-mode scaling validated at JET[11] was used for the second phase. The methodology was tested on JET discharges[20]. Fueling was adjusted to match separatrix density; pumping was set to  $50\,\mathrm{m}^3/\mathrm{s}$  in scenario A and  $100\,\mathrm{m}^3/\mathrm{s}$  in scenario E. Impurity seeding was tested using oxygen as a proxy for mid-Z species, calibrated to Zeff  $\simeq 1.3$ . The current first wall geometry[21][22], under axys-symmetric approximation, was implemented.

Flat-top phases were modelled for scenarios A, C, and E. Target separatrix densities were prescribed from previous modelling campaigns and scaled with the Greenwald fraction where appropriate[23]. The power crossing the separatrix was set to 6 MW (A), and 30 MW (E), with a 60/40 ion/electron partition as from ASTRA simulations. Heat transport coefficients were derived from Eich's scaling[10] scaled to DTT [24]. To achieve outer divertor detachment, impurity seeding was applied: nitrogen for A and neon or argon for E. Detached initial conditions were assumed to avoid hysteresis effects.

#### 4.1. Scenario A

Edge simulations for Scenario A, covering both ramp-up and flat-top phases, confirm the overall consistency with core modelling predictions. Edge transport parameters evaluated from scaling laws and from ASTRA were very similar. Figures 3a and 3b show the electron temperature at the inner limiter, inner, outer target and at LCFS, which are very similar between ASTRA and scaling laws because transport parameter estimations are very similar. SOLEDGE2D–EIRENE produced more peaked density profiles than ASTRA, likely due to an underestimation of neutral penetration in the core-only simulations, which do not fully capture recycling and neutral-plasma interactions. During the limiter phase, SOLEDGE systematically predicted lower separatrix electron temperatures than ASTRA, suggesting that resistivity and loop voltage consumption may have been slightly underestimated in the core model; although, voltage usage is not a major concern for scenario A due to lower density and impurity concentration than other scenarios.





(a) Scenario A  $T_e$  peak at the inner limiter, inner target and outer target during the ramp-up with different transport parameter assumptions.

(b) Scenario A  $n_e$  and  $T_{e,sep}$  ramp-up with different transport parameter assumptions.

FIG. 3. SOLEDGE output for scenario A ramp-up.

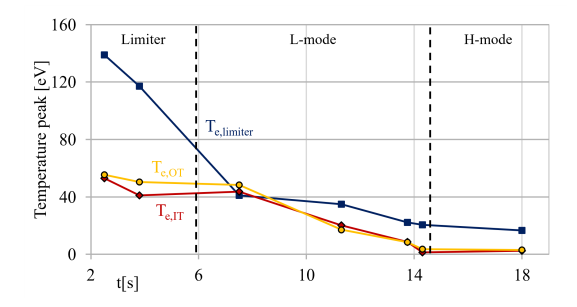
Thermal loads on the plasma-facing components were found to remain well below engineering limits throughout the discharge. Maximum wall heat fluxes were estimated at around  $0.5\,\mathrm{MW/m^2}$ , while electron temperatures at the inner limiter peaked at  $\sim 80\,\mathrm{eV}$ . These values are consistent with experimental observations at JET in comparable ramp-up phases and confirm that Scenario A provides a safe operational regime for the commissioning stage of DTT.

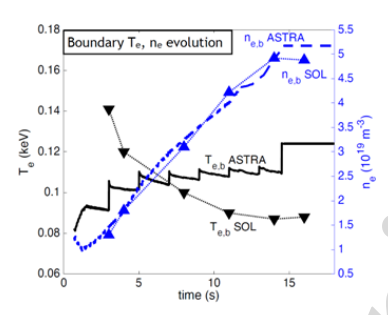
Impurity seeding tests using oxygen demonstrated that controlled radiative cooling can be achieved already during ramp-up. However, excessive injection led to premature radiative collapse, pointing to the need for careful feedback control of impurity concentration. Therefore, in Scenario A, seeding during the early discharge should be minimised, relying mainly on intrinsic impurities, while deliberate impurity injection should be reserved for the flat-top phase. In this latter regime, nitrogen injection proved effective in producing deep detachment, with the recombination front located well upstream of the divertor targets. Importantly, plasma purity remained high, with  $Z_{\rm eff} \simeq 1.3$ , demonstrating that efficient power exhaust can be achieved without compromising core performance. These results show that Scenario A offers wide operational margins, enabling long-pulse, impurity-tolerant discharges that are well suited for developing plasma control strategies.

#### 4.2. Scenario E

In Scenario E, edge simulations confirm that detached divertor operation is also feasible, but with narrower margins compared to Scenario A. During the ramp-up, SOLEDGE confirmed the overall plausibility of the ASTRA-predicted trajectories but revealed that empirical scalings tend to overestimate transport coefficients at the separatrix. Fig. 4a and 4b show the output of SOLEDGE modelling, using the shortest estimation of profiles (derived from ASTRA), which produce the highest T<sub>e</sub> estimation. This behaviour can be attributed to the limited availability of experimental data at high toroidal field and density, typical of reactor-relevant conditions. Nevertheless,

thermal loads on the first wall and limiters remained within acceptable limits, and separatrix electron temperatures stayed compatible with material constraints, although close to critical values in the most demanding phases.





(a) Scenario E  $T_e$  peak at the inner limiter, inner target and outer target during the ramp-up.

(b) Scenario A  $n_e$  and  $T_{e,sep}$  rampup.

FIG. 4. SOLEDGE output for scenario E ramp-up.

Flat-top conditions in Scenario E required significantly higher impurity levels to achieve divertor detachment. Neon seeding proved particularly effective, yielding strong detachment with the recombination front extending close to the X-point. This deep detachment offers operational flexibility, as impurity levels or separatrix density could be reduced while maintaining safe thermal conditions. At the same time, the risk of impurity penetration into the confined plasma is higher than in Scenario A, highlighting the importance of optimising seeding strategies in real time.

Radial profile analysis revealed clear differences between nitrogen and neon transport: nitrogen remained largely confined to the divertor region, whereas neon penetrated more deeply, leading to broader  $Z_{\rm eff}$  distributions. This behaviour is consistent with previous modelling campaigns and suggests that, while neon is more effective at achieving detachment, it requires stricter monitoring of core impurity content. Overall, Scenario E confirms that the DTT divertor can handle reactor-relevant heat fluxes with proper seeding strategies, but it also emphasises the need for accurate real-time control systems to balance detachment, confinement, and impurity management.

## 5. PLASMA-WALL INTERACTION MODELLING

The modelling of plasma-wall interactions is performed through the Monte Carlo code ERO2.0, which allows for a kinetic treatment of impurity transport starting from the erosion of plasma-facing components (PFCs). In section 5.1, the ramp-up phase is described in limiter configuration. In section 5.2, the flat top phase is modelled, including the ELM effect.

ERO 2.0 used SOLEDGE plasma background, ensuring self-consistent input conditions in terms of electron density, temperature, ion temperature, parallel velocity, and magnetic field geometry. The code tracks eroded particles using both the Guiding Centre Approximation (GCA) and full orbit trajectories, in order to assess the role of approximations in predicting impurity migration from the wall to the core plasma.

Four instants of the limiter phase were studied:  $t=1.25\,\mathrm{s}$  for early ramp-up, low current, plasma in limiter configuration,  $t=2.5\,\mathrm{s}$  for intermediate ramp-up, increased current, still limiter-dominated interaction,  $t=3.75\,\mathrm{s}$  late ramp-up, before transition to diverted configuration and a flat top instant. L-mode phase gives less concern than the H-mode phase and was not considered in this study.

For the three limited cases, the background plasma parameters were evaluated in both high-transport and low-transport cases. In the high-transport case, the edge plasma is colder and denser, lowering sputtering, whereas in the low-transport case, hotter edge conditions are expected, increasing erosion rates. This dual-case approach provided a sensitivity analysis of how boundary conditions affect impurity generation and migration.

The simulations considered both D-only plasma discharges and oxygen-seeded cases, motivated by previous observations of oxygen release in tungsten machines such as WEST[3]. Oxygen is also a proxy for all intrinsic mid-Z impurities. The role of tungsten (originating from the first wall and divertor) was also systematically investigated, since even trace amounts can critically affect Vloop usage and core plasma performance.

## 5.1. Scenario E Ramp-up

Particular attention was paid to the limiter phase, as excessive tungsten erosion in this phase can hurt the entire discharge (WEST). For this reason, specific attention is devoted to shadowing effects, i.e. how geometric features of the limiter protect or expose regions to plasma fluxes, and to the influence of grazing angles on sputtering yields.

The simulations also include extrinsic impurity sources, such as oxygen, to reproduce experimentally observed contamination scenarios in metallic machines (e.g. WEST)[3].

For the ramp-up analysis, the plasma was assumed to be in contact with the inner first wall limiter. The simulations explored the effect of shadowing; that is, multiple limiter geometrical configurations were studied in the limiter design process. The axys-symmetric limiter, a configuration with 36 poloidal limiters with  $5^{\circ}$  step, 18 limiters with  $10^{\circ}$  steps and 9 limiters with  $10^{\circ}$  steps[25]. The current geometry is made of 18 poloidal limiters separated by  $10^{\circ}$  angle [21][22].

Rather than implementing a fully three-dimensional reconstruction of the wall geometry, which would have required prohibitive computational resources within the Monte Carlo framework of ERO2.0, a conservative assumption of a fixed incidence angle of  $60^{\circ}$  was adopted. This choice is consistent with previous kinetic and PIC-based studies[26], which have shown that sputtering yields increase significantly at grazing incidence and that values around  $60^{\circ}$  can be considered representative of limiter-plasma interactions in metallic devices. In addition to this approach, specific simulations were carried out without this constraint. This procedure enabled the evaluation of how sensitive the source of the impurity and subsequent core contamination are to assumptions about particle impact geometry[25].

Fig. 5 shows the radial profile of the estimated tungsten concentration for the different geometries in the cases obtained from the simulated background plasma with minor transport profiles. To avoid redundancies, cases with higher transport profiles are omitted. Erosion is threefold in cases with minor transport profiles, which can be considered worst-case scenarios. A time trace of the tungsten density will be shown in section, also including the flat-top results.

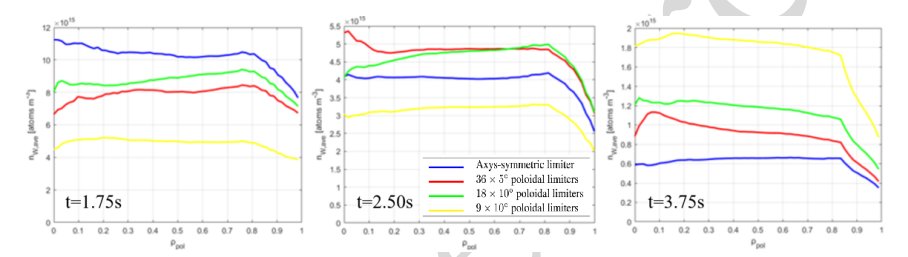


FIG. 5. Tungsten density radial profile during the ramp-up obtained with different limiter geometries.

Tungsten concentration does not drastically increase with time, even if particle flux to the wall increases. Lastly, core contamination is affected by the shape of limiters; the trend is unclear at lower current, but at higher current, the higher the number of limiters, the lower the W content.

If intrinsic impurities are included in the modelling, using oxygen as a proxy for mid-Z impurities as described in section 4, W content increases by a factor of three as shown in figure 5. It should be noted that ASTRA modelling assumed a  $10^{-5}$  W concentration at the separatrix, which is higher than that estimated by PWI modelling; thus demonstrating that the core modelling assumptions were conservative.

# 5.2. Scenario E flat-top

Two reference plasma conditions were used as plasma background: an attached pure deuterium case ( $P_{sol}=14$  MW,  $n_{e,sep}=7\times10^{19}\,\text{m}^{-3}$ ) and a detached case with neon seeding ( $P_{sol}=27\,\text{MW}$ ,  $n_{e,sep}=8\times10^{19}\,\text{m}^{-3}$ ). Plasma backgrounds were imported from SOLEDGE calculations (see section 4.2) and used as inputs for a  $20^{\circ}$  toroidally symmetric 3D sector of the divertor. The analysis included a scan of ion incidence angles ( $30^{\circ}-70^{\circ}$ ), the effect of oxygen impurities (2% concentration), and the role of ELMs, modeled as periodic bursts of  $D^+$  ions (10-30 Hz, pedestal-top temperature  $\sim 1$  keV) applied either locally at the outer strike point (OSP) or across the whole outer divertor (OD). Results are summarized in table 2

In ELM-free conditions, net erosion rates were found to remain below  $10^{-3}$  nm/s for both attached and detached plasmas (Tab.2). This indicates that baseline operation is characterised by a very limited W source. The inclusion of oxygen impurities strongly enhanced erosion by approximately one order of magnitude in the attached case and by a factor of 6–7 in the detached case. These results highlight the strong dependence of divertor erosion on extrinsic impurity content.

The presence of ELMs further increased erosion, producing peak rates up to  $0.5 \, \mathrm{nm/s}$  during the intra-ELM phase (Tab.2). While these values exceed those in steady-state conditions, they remain within an acceptable operational range, below observed rates[27]. Prompt redeposition processes were found to be significant, particularly in the attached scenario where higher local electron temperatures favour rapid recycling of eroded W to nearby surfaces. From the perspective of core contamination, DTT shows robust screening properties. Even in the most extreme assumption of energetic  $D^+$  bursts over the entire outer divertor, the simulated W density reaching the confined

plasma remained below established limits for all anomalous cross-field diffusion coefficients considered  $(0.1-10 \text{ m}^2/\text{s})$  (Fig. 5).

Overall, these results suggest that the DTT divertor is expected to operate in a net erosion regime with limited risk of tungsten core penetration, even in scenarios including ELM activity and conservative impurity assumptions. Nevertheless, some uncertainties remain due to model simplifications, such as the treatment of ELMy conditions in ERO2.0, the neglect of charge-exchange neutrals, and the absence of divertor block shaping. These aspects should be addressed in future studies to consolidate the robustness of the present predictions.

TABLE 2. SUMMARY OF EROSION AND CORE CONTAMINATION RESULTS FOR DTT SCENARIO E.

Sc. E conditions	Condition	Net erosion rate	c <sub>W,sep</sub> (part/m <sup>3</sup> )	c <sub>W,core</sub> (part/m <sup>3</sup> )
t = 1.25  s	D only	$2.0\mathrm{nm/s}$	$3.9 \times 10^{15}$	$4.2 \times 10^{15}$
$t = 2.5 \mathrm{s}$	D only	$1.0\mathrm{nm/s}$	$2.0 \times 10^{15}$	$2.9 \times 10^{15}$
$t = 3.75 \mathrm{s}$	D only	$0.4\mathrm{nm/s}$	$0.9 \times 10^{15}$	$1.3 \times 10^{15}$
Attached (D)	2% O, w/ ELMs	Up to 0.5 nm/s	$\leq 10^{12}$	$\leq 10^{12}$
Detached (D+Ne)	2% O, w/ ELMs	Up to 0.5 nm/s	$\leq 10^{12}$	$\leq 10^{12}$
Extreme case	D <sup>+</sup> burst over OT	$\sim$ 0.5 nm/s	$\leq 10^{14}$	$\leq 10^{14}$

Tab. 2 lists the estimated tungsten density in the main plasma and at the separatrix during the ramp-up of scenario E, which is similar to that assumed for core modelling and should guarantee the expected performance of the machine. These results demonstrate that the most critical phase for limiting impurity content is the limiter phase, since the highest W contamination is produced in that phase.

#### 6. CONCLUSIONS

This work has presented an integrated modelling study of DTT operational scenarios in a full-metallic environment, combining core transport, edge plasma behaviour, and plasma-wall interaction. The coordinated use of METIS, ASTRA, CREATE-NL, SOLEDGE2D-Eirene, and ERO2.0 enabled a self-consistent assessment of discharge evolution from ramp-up to H-mode operation. For Scenario A, simulations demonstrated the feasibility of long-pulse operation with moderate auxiliary heating, stable confinement, and safe thermal loads on plasmafacing components. The L-H transition was achieved with limited flux consumption, ensuring extended flat-top durations compatible with experimental needs. For Scenario E, operation under reactor-relevant conditions was shown to be feasible, provided careful optimisation of the ramp-up and auxiliary heating scheme is applied to control current profiles, limit impurity accumulation, and preserve MHD stability. Edge modelling confirmed the capability to achieve detached divertor operation across all scenarios, with impurity seeding requirements reduced compared to earlier designs. Nitrogen and neon seeding were shown to provide effective detachment while maintaining high plasma purity. Plasma-wall interaction analysis further indicated that tungsten erosion and core contamination remain within acceptable limits, even in the presence of ELMs and extrinsic impurities, thanks to the robust screening properties of the DTT divertor; the limiter phase is the most critical in terms of tungsten accumulation. Overall, the study confirms that properly designed operational scenarios enable DTT to achieve its mission of addressing power exhaust and plasma-wall interaction challenges in metallic environments. The results provide confidence that DTT will serve as a key platform for ITER and DEMO-relevant investigations, while also highlighting the importance of continued modelling and experimental validation, particularly regarding limiter geometry effects, impurity migration, and ELM-induced erosion.

#### REFERENCES

- [1] F. ROMANELLI and on behalf of DTT Contributors. In: *Nuclear Fusion* 64.11 (Sept. 2024), p. 112015. DOI: 10.1088/1741-4326/ad5740.
- [2] F. CRISANTI et al. In: Nuclear Fusion 64.10 (Sept. 2024), p. 106040. DOI: 10.1088/1741-4326/ad6e06.
- [3] P. MAGET et al. In: *Plasma Physics and Controlled Fusion* 64.4 (Feb. 2022), p. 045016. DOI: 10.1088/1361-6587/ac4b93.
- [4] N. BONANOMI et al. In: Nuclear Fusion 65.1 (Nov. 2024), p. 016005. DOI: 10.1088/1741-4326/ad8edb.
- [5] I. CASIRAGHI et al. In: *Plasma Physics and Controlled Fusion* 65.3 (Feb. 2023), p. 035017. DOI: 10.1088/1361-6587/acb6b1.
- [6] C. BACKMANN et al. In: Fusion Engineering and Design 204 (2024), p. 114518. ISSN: 0920-3796. DOI: https://doi.org/10.1016/j.fusengdes.2024.114518.

#### L. BALBINOT et al.

- [7] R. ALBANESE, R. Ambrosino, and M. Mattei. In: Fusion Engineering and Design 96-97 (2015). Proceedings of the 28th Symposium On Fusion Technology (SOFT-28), pp. 664–667. ISSN: 0920-3796. DOI: https://doi.org/10.1016/j.fusengdes.2015.06.162.
- [8] J.F. ARTAUD et al. In: Nuclear Fusion 58.10 (Aug. 2018), p. 105001. DOI: 10.1088/1741-4326/aad5b1.
- [9] A. STANGEBY. Bristol: Institute of Physics, (2000).
- [10] T. EICH et al. In: Nuclear Fusion 53.9 (Aug. 2013), p. 093031. DOI: 10.1088/0029-5515/53/9/093031.
- [11] A. SCARABOSIO et al. In: *Journal of Nuclear Materials* 438 (2013). Proceedings of the 20th International Conference on Plasma-Surface Interactions in Controlled Fusion Devices, S426–S430. ISSN: 0022-3115. DOI: https://doi.org/10.1016/j.jnucmat.2013.01.086.
- [12] R.J. GOLDSTON. In: Nuclear Fusion 52.1 (Dec. 2011), p. 013009. DOI: 10.1088/0029-5515/52/1/013009.
- [13] G.V. PEREVERZEV et al. IPP-5/42. Garching (Germany): Max-Planck-Institut fuer Plasmaphysik, (1991).
- [14] F. FRANZA et al. In: Nuclear Fusion 62.7 (June 2022), p. 076042. DOI: 10.1088/1741-4326/ac6433.
- [15] H. BUFFERAND et al. In: Nuclear Fusion 55.5 (Apr. 2015), p. 053025. DOI: 10.1088/0029-5515/55/5/053025.
- [16] H. BUFFERAND et al. In: *Journal of Nuclear Materials* 438 (2013). Proceedings of the 20th International Conference on Plasma-Surface Interactions in Controlled Fusion Devices, S445–S448. ISSN: 0022-3115. DOI: https://doi.org/10.1016/j.jnucmat.2013.01.090.
- [17] J. ROMAZANOV et al. In: Nuclear Fusion 64.8 (June 2024), p. 086016. DOI: 10.1088/1741-4326/ad5368.
- [18] M. KOCAN et al. In: *Nuclear Fusion* 55 (Mar. 2015), p. 033019. DOI: 10.1088/0029-5515/55/3/033019.
- [19] J. HORACEK et al. In: *Plasma Physics and Controlled Fusion* 58.7 (May 2016), p. 074005. DOI: 10.1088/0741-3335/58/7/074005.
- [20] C. MEINERI and et al. Scientific report. Frascati (Italy): DTT Scarl, (2021).
- [21] M. FURNO PALUMBO et al. In: Fusion Engineering and Design 222 (2026), p. 115435. ISSN: 0920-3796. DOI: https://doi.org/10.1016/j.fusengdes.2025.115435.
- [22] S. ROCCELLA. Presented at this conference. This conference. 30th IAEA Fusion Energy Conference (IAEA FEC 2025), (2025).
- [23] L. BALBINOT, G. Rubino, and P. Innocente. In: *Nuclear Materials and Energy* 27 (2021), p. 100952. ISSN: 2352-1791. DOI: https://doi.org/10.1016/j.nme.2021.100952.
- [24] L. BALBINOT et al. In: *Nuclear Materials and Energy* 34 (2023), p. 101350. ISSN: 2352-1791. DOI: https://doi.org/10.1016/j.nme.2022.101350.
- [25] F. CANI and et al. 66th Annual Meeting of the APS Division of Plasma Physics. Conference proceedings. Atlanta, Georgia, (2025).
- [26] F. CICHOCKI et al. In: *Plasma Physics and Controlled Fusion* 66.2 (Jan. 2024), p. 025015. doi: 10.1088/1361-6587/ad1a41.
- [27] A. HAKOLA et al. In: Nuclear Fusion 61.11 (Sept. 2021), p. 116006. DOI: 10.1088/1741-4326/ac22d2.